JACS
JOURNAL OF THE AMERICAN CHEMICAL SOCIETY
Article
pubs.acs.org/JACS

Mechanistic Evaluation of Motion in Redox-Driven Rotaxanes Reveals Longer Linkers Hasten Forward Escapes and Hinder Backward Translations

Sissel S. Andersen,[†,‡] Andrew I. Share,[‡] Bjørn La Cour Poulsen,[†] Mads Kørner,[†] Troels Duedal,[†] Christopher R. Benson,[‡] Stinne W. Hansen,[†] Jan O. Jeppesen,*[,†] and Amar H. Flood*[,‡]

[†]Department of Physics, Chemistry, and Pharmacy, University of Southern Denmark, Campusvej 55, 5230 Odense M, Denmark
[‡]Department of Chemistry, Indiana University, 800 East Kirkwood Avenue, Bloomington, Indiana 47405, United States

Supporting Information

ABSTRACT: Mechanistic understanding of the translational movements in molecular switches is essential for designing machine-like prototypes capable of following set pathways of motion. To this end, we demonstrated that increasing the station-to-station distance will speed up the linear movements forward and slow down the movements backward in a homologous series of bistable rotaxanes. Four redox-active rotaxanes, which drove a cyclobis(paraquat-*p*-phenylene) ($CBPQT^{4+}$) mobile ring between a tetrathiafulvalene (TTF) station and an oxyphenylene station, were synthesized with only variations to the lengths of the glycol linker connecting the two stations (n = 5, 8, 11, and 23 atoms). We undertook the first mechanistic study of the full cycle of motion in this class of molecular switch using cyclic voltammetry. The kinetics parameters (k, $\Delta G^{\ddagger}$) of switching were determined at different temperatures to provide activation enthalpies ($\Delta H^{\ddagger}$) and entropies ($\Delta S^{\ddagger}$). Longer glycol linkers led to modest increases in the forward escape ($t_{1/2}$ = 60 to <7 ms). The rate-limiting step involves movement of the tetracationic $CBPQT^{4+}$ ring away from the singly oxidized TTF^{+} unit by overcoming one of the thiomethyl (SMe) speed bumps before proceeding on to the secondary oxyphenylene station. Upon reduction, however, the return translational movement of the $CBPQT^{4+}$ ring from the oxyphenylene station back to the neutral TTF station was slowed considerably by the longer linkers ($t_{1/2}$ = 1.4 to >69 s); though not because of a diffusive walk. The reduced rate of motion backward depended on folded structures that were only present with longer linkers.

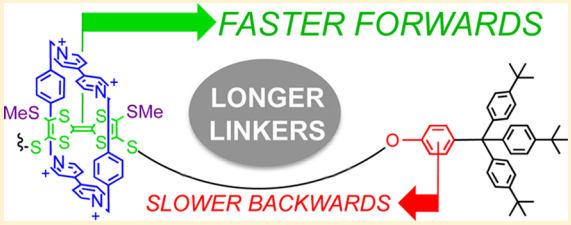

INTRODUCTION

Biological molecular machines rely upon the regulation of chemical processes,[1] among others, to ensure a specific sequence[2] of events is followed in order for work done in one movement not be undone in the next. Consequently, the precise timing of each step in the cycle of motion is vital for performing work and achieving unidirectional movements.[3] Synthetic molecular switches and machines have been synthesized and studied[3] as a means to mimic these underlying principles.[4] Yet, the vast majority of these investigations have focused on identifying ways to control the thermodynamics of motion.[3,5] Considering rotaxanes as exemplary,[6−9] this outcome has been highly successful and is now characterized by the almost predictable[5,10−13] control over the reversible linear motion of a ring component between primary and secondary stations along the dumbbell, a property called bistability. The thermodynamic character of the resulting linear movements, however, is inherently path independent. One way to better mimic the behaviors of biomachines is to instead develop an understanding of path-dependent properties;[14−17] such as establishing knowledge of how molecular structure impacts the kinetics of motion.[11,18] Mechanistic studies, therefore, are essential[19−23] for developing and testing strategies on how to control, gate, and modulate movements in molecular machines and motors. Despite their importance, there are still only a few studies[11,18,24−28] aiming to elucidate the microscopic details of the pathways of motion in bistable interlocked molecules. There are even fewer studies[21,22,29] that characterize a complete cycle both forward and backward; none of which involve the systems of tetrathiafulvalene (TTF) and cyclobis(paraquat-*p*-phenylene) ($CBPQT^{4+}$).

A number of strategies have been investigated to understand and control the rates of motion in rotaxanes[6,7] and catenanes.[30,31] One approach has involved changing and tuning the stations[11,18] where deeper potential wells slow molecular movements. Such modifications often have the undesired effect of influencing the thermodynamics and, consequently, the Boltzmann-weighted change in populations during switching. More direct efforts[22] to control kinetics have utilized large bulky groups to completely block the pathway between two stations. Steric-based speed bumps,[17,24,25,33] redox-switchable electrostatic speed bumps,[27,34] photoswitchable gates and dynamic foldameric linker regions[28] have also been employed to control the kinetics of motion. In an

Received: February 8, 2014
Published: April 18, 2014

   dx.doi.org/10.1021/ja5013596 | J. Am. Chem. Soc. 2014, 136, 6373−6384

analogous manner, modulating the size of the mobile ring has been found to have a significant effect on the kinetics of switching in rotaxanes.[29,35,36] An alternative approach involves modifications to the length of the native linker[26,37,38] that connects the two different stations together.

An exemplary study by Leigh[26] made use of time-resolved vibrational spectroscopy[39] to watch the departure and arrival of a mobile ring between the two stations in a series of amide-derived, hydrogen-bonded bistable rotaxanes. The probability of the ring moving forward to the secondary station was found to be split into two kinetically resolved processes: First, escape from the primary station required thermal activation. Second, the probability of the ring stepping forward or backward along the alkyl linker region with n = 5, 9, 12, or 16 methylene units was based on a diffusive, yet biased, random walk along a one-dimensional pathway. When longer linkers (n = 16) were used, the net probability of the ring moving to the second station became smaller, resulting in slower kinetics of switching for this step and for the entire process. The slowing of the rates with increasing linker length has also been observed in the threading and dethreading of a macrocycle along a polymer chain bearing a viologen station.[37] While the diffusive walks in these cases contributed to the observed rates, it has also been proposed that the thermally activated escape from the initial station will dominate[26] the rate behavior in interlocked molecules. Thus, there exist two alternative ideas regarding the rate-limiting steps (RLSs) of translational movements in rotaxanes that can best be distinguished using mechanistic studies.

One of the most studied and reliable set of molecular switching gear is based on the interaction between the redox active TTF unit and the CBPQT^{4+} ring.[6,11,24,30,32,40] Flexible ethylene glycol linkers are almost exclusively employed to connect the TTF unit to other stations on account of their ability to aid[41] in the template-directed synthesis of rotaxanes. These linkers also help stabilize the CBPQT^{4+} ring once it is localized at a station, i.e., they participate in the thermodynamic stabilization of one station over another.[11] Few studies,[23,42] however, have been directed at examining their role in the mechanisms of redox-driven motion. Furthermore, within the class of TTF–CBPQT^{4+} rotaxanes, the mechanisms of motion for both the forward and backward switching are usually studied in separate compounds; the mechanism of a complete cycle has yet to be examined across a homologous series.

Herein, we characterize the impact of the ethylene glycol linker lengths on the translational motion forward and backward within a series of rotaxanes. We have measured the kinetics of motion for a complete cycle (Scheme 1) using bistable rotaxanes $\mathbf{R_S}^{4+}$, $\mathbf{R_M}^{4+}$, $\mathbf{R_L}^{4+}$, and $\mathbf{R_{XL}}^{4+}$ (Figure 1) with short (S), medium (M), long (L), and extra long (XL) glycolic linkers composed of 5, 8, 11, and 23 atoms, respectively. In this class of rotaxanes, it is known[43] that oxidation of the TTF unit (green) to TTF^{+} is sufficient to repel the tetracationic CBPQT^{4+} ring (blue) causing it to move to a secondary station (red). Subsequent oxidation to TTF^{2+} generates the switched rotaxane, **SR**$^{6+}$. Full reduction back to the neutral TTF station removes all electrostatic repulsions and allows the macrocycle to return to its initial position (Scheme 1). Herein, switching was characterized by ^{1}H NMR spectroscopy to confirm the location of the CBPQT^{4+} ring in the switched state for each rotaxane. During these investigations it was also discovered that oxyphenylenes located on the stoppers act as secondary stations. The location of the mobile rings and the associated conformations of the switched rotaxane **SR**$^{6+}$ and metastable intermediate **SR**$^{4+}$ were characterized structurally using NMR spectroscopy on control compounds also as a function of chain length. Cyclic voltammetry (CV) was recorded at fast and slow scan rates and then simulated to characterize kinetics (k) and activation parameters ($\Delta G^{\ddagger}$, $\Delta H^{\ddagger}$, $\Delta S^{\ddagger}$) of switching. The effects of the linker's length on the kinetics gave evidence for the mechanism of motion in this class of rotaxane. In contrast to Leigh's findings,[26] the movement of the ring in the forward direction was hastened modestly when the linker was extended in length while the return motion was slowed considerably. We observe rates that are largely limited by the thermally activated escape from either the primary or secondary stations. Unlike Leigh's findings, net rates of motion forwards or backwards are too small to reveal any biased random walks. Nevertheless, these movements still display a dependence on the length of the linker. Overall, these findings indicate that the linker's length can influence the escape energy and thus the microscopic details of motion just as it can in a diffusive random walk between stations.

Scheme 1. Overall Cycle of Voltage-Driven Switching in TTF–CBPQT^{4+} Rotaxanes[a]

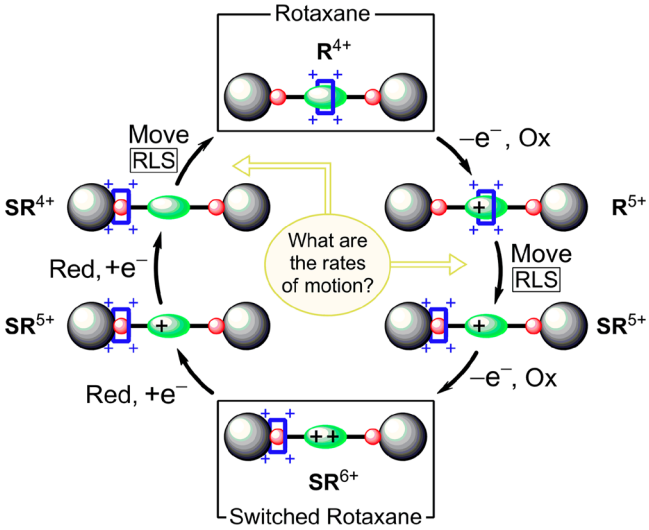

[a]The overall switching cycle starting from rotaxane $\mathbf{R}^{4+}$ (top) involves oxidation to $\mathbf{R}^{5+}$ that is followed by switching to $\mathbf{SR}^{5+}$ which is almost always oxidized immediately to $\mathbf{SR}^{6+}$ when the rotaxanes are under voltage control. The switched rotaxane $\mathbf{SR}^{6+}$ is reduced in two steps to $\mathbf{SR}^{4+}$ which allows molecular movements of the ring (blue) to reinstate rotaxane $\mathbf{R}^{4+}$.

RESULTS AND DISCUSSION

Molecular Design. Studies, presented herein, revealed the two identical oxyphenylenes (red, Figure 1) act as secondary stations to complement the primary redox-active TTF station. The outcome is a three-station, bistable rotaxane capable of switching left or right with equal probability. Within each rotaxane, thiomethyl groups (SMe, purple, Figure 1) were incorporated on either side of the central TTF station to slow the movements down such that the rates forward (<60 ms) and backward (>1 s) could both be quantified with electrochemical methods by using a range of temperatures (263–333 K) and scan rates (166–0.2 V s^{-1}). The linkers are extended by one ethylene glycol across the short, medium, and long rotaxanes, while they double in length from short to long to extra long rotaxanes. Using electrogenerated TTF^{+}, we can watch the escape of the mobile ring in the forward direction, however, we cannot observe its

dx.doi.org/10.1021/ja5013596 | J. Am. Chem. Soc. 2014, 136, 6373–6384

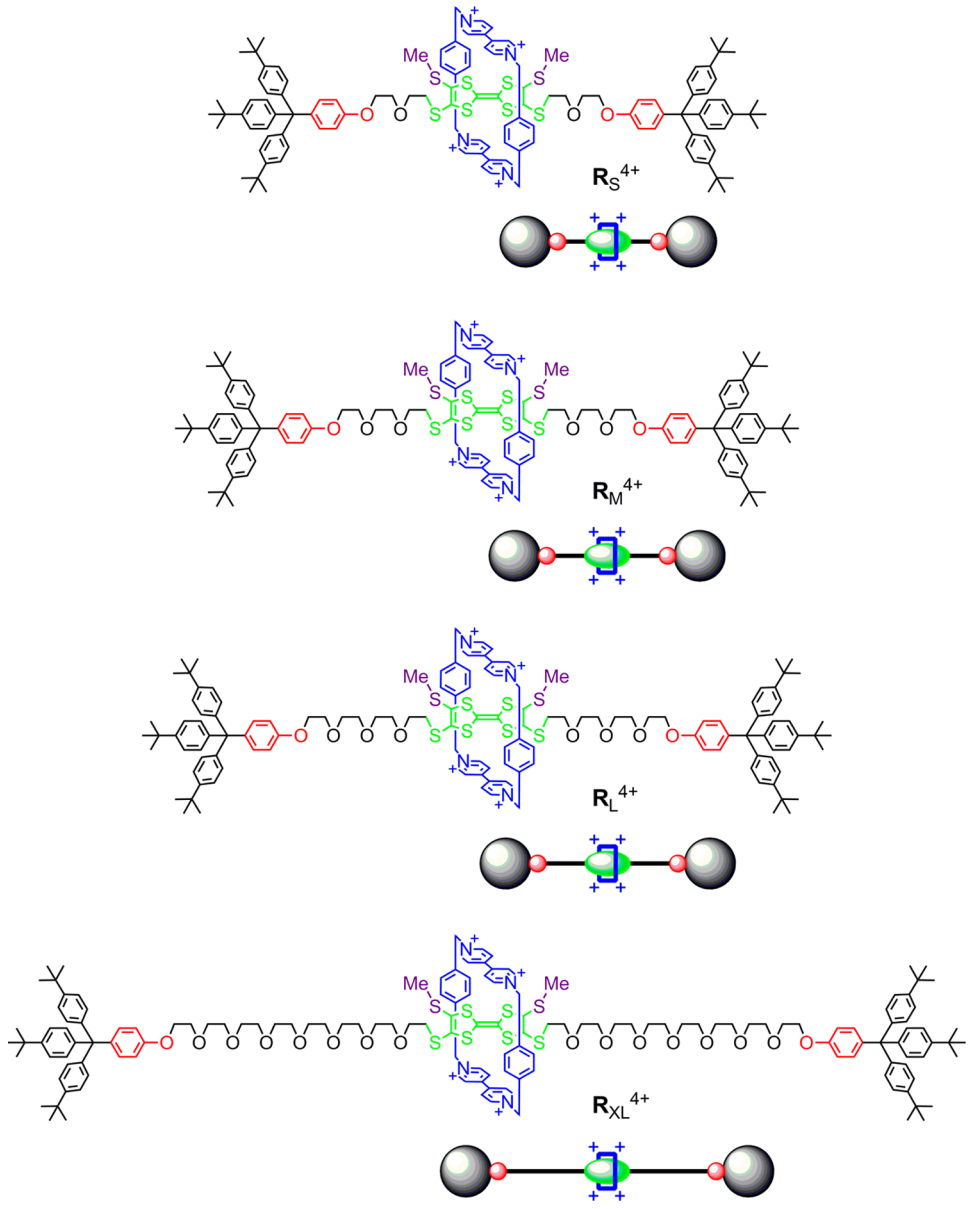

Figure 1. Molecular structure and cartoon representations of [2]rotaxanes $\mathbf{R}_S^{4+}$, $\mathbf{R}_M^{4+}$, $\mathbf{R}_L^{4+}$, and $\mathbf{R}_{XL}^{4+}$.

arrival at the secondary station by electrochemical means. By contrast, the times of departure and arrival can be reliably measured for the return movement.

Synthesis. The four different dumbbells that are precursors to $\mathbf{R}_S^{4+}$, $\mathbf{R}_M^{4+}$, $\mathbf{R}_L^{4+}$, and $\mathbf{R}_{XL}^{4+}$ were all synthesized in a similar fashion from the *cis*/*trans* mixture of the same TTF derivative,[44] the same bulky tetraaryl stopper,[45] and four glycols of different lengths with 5, 8, 11, and 23 atoms. The TTF unit served as a template for the formation of the tetracationic $CBPQT^{4+}$ ring around the dumbbell from the dicationic precursor[46] and 1,4-bis(bromomethyl)-benzene. The dumbbells and rotaxanes were characterized by NMR spectroscopy, mass spectrometry, and elemental analyses (see Supporting Information).[47]

Chemical Switching Studies using ^{1}H NMR Spectroscopy. In order to investigate the location of the ring in the switched state, $\mathbf{SR}^{6+}$, ^{1}H NMR spectroscopy was used to monitor the changes to the hydrogen environments upon addition of 10 equiv of the chemical oxidant tris-*p*-bromophenylammoniumyl hexachloroantimonate ($TBPASbCl_6$).[48] Initially all four rotaxanes had similar ^{1}H NMR spectra (Figure S1), indicating they have similar structures. Following oxidation, the observations of significant shifts to all of the protons in the spectra were consistent with switching.[49−52] The new location of the $CBPQT^{4+}$ ring along the dumbbell of each rotaxane was readily determined from the strong shielding felt by the oxyphenylene protons when they are encircled by the ring (e.g., H_a and H_b, Figure 2).

In the ^{1}H NMR spectrum of the switched rotaxane bearing the short linker, $\mathbf{SR}_S^{6+}$ (Figure 2c), the protons associated with the SMe speed bumps are shifted downfield (δ = 2.92 and 2.87 ppm) relative to the position at which they are found to resonate in the parent rotaxane, $\mathbf{R}_S^{4+}$ (δ = 2.58 ppm, Figure 2b). Previous investigations have shown that such behavior is entirely consistent with the formation of the TTF^{2+} dication[49,50] and, therefore, of the oxidized rotaxane. The inequivalence in their positions is indicative of the lower symmetry in $\mathbf{SR}_S^{6+}$ in which the $CBPQT^{4+}$ has moved away from TTF^{2+}. Evidence for the linear translation of the ring to encircle one of the O-linked

dx.doi.org/10.1021/ja5013596 | *J. Am. Chem. Soc.* 2014, 136, 6373−6384

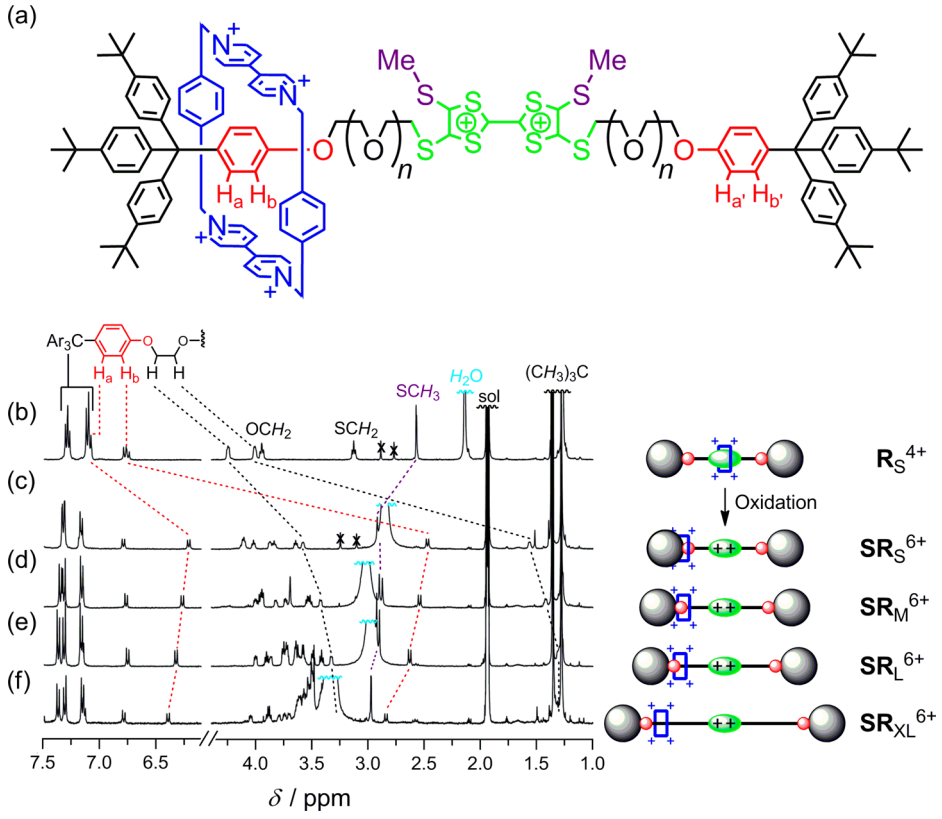

Figure 2. (a) The structure of $\mathbf{SR}^{6+}$ with hydrogen labels. Partial ^{1}H NMR spectra (400 MHz, 298 K, CD_3CN, 2.0 mM) of (b) $\mathbf{R}_S^{4+}$, (c) $\mathbf{SR}_S^{6+}$, the signal from one of the SMe groups (i.e., δ = 2.87 ppm) is obscured under the H_2O signal (broad signal around ~2.8 ppm), (d) $\mathbf{SR}_M^{6+}$, (e) $\mathbf{SR}_L^{6+}$, and (f) $\mathbf{SR}_{XL}^{6+}$. The switched rotaxanes $\mathbf{SR}_i^{6+}$ (i = S, M, L, and XL) are all generated by adding 10 equiv of the oxidant $TBPASbCl_6$. The signals being crossed out arise from traces of DMF present in the samples after the synthesis.

oxyphenylene stations is made obvious from the dramatic changes (Figure 2c) of the chemical shift position of that particular O-linked oxyphenylene's H_a and H_b protons. In the starting rotaxane $\mathbf{R}_S^{4+}$, the resonances appear at δ = 7.10 ppm (H_a) and δ = 6.77 ppm (H_b). Upon oxidation, the signals for one of the oxyphenylene stations experience large upfield shifts to δ = 6.22 ppm (H_a) and δ = 2.48 ppm (H_b) on account of the anisotropic shielding effect (Figure 2c) that occurs when the $CBPQT^{4+}$ ring encircles that station. The significant upfield shift ($\Delta\delta$ = 4.29 ppm) of the oxyphenylene's H_b protons can most likely be explained by the fact that they participate in C−H···π interactions with the $CBPQT^{4+}$ ring by pointing toward the faces of the *p*-xylene units of $CBPQT^{4+}$. The signals for the other oxyphenylene station remain almost at the original positions (δ = 7.18 and 6.80 ppm for $H_{a'}$ and $H_{b'}$, respectively). Examination of the ^{1}H correlation spectroscopy (COSY) spectrum for $\mathbf{SR}_S^{6+}$ recorded in CD_3CN at 298 K (Figure S3) clearly shows the through-bond scalar coupling between the two shielded protons in the oxyphenylene station. Consistently, the protons associated with the two methylene groups (−O−CH_2−CH_2−) attached directly to the encircled oxyphenylene station in $\mathbf{SR}_S^{6+}$ are similarly shielded (Figure 2c) and display through-bond scalar coupling (Figure S3). Taken all together, these observations unambiguously show that the $CBPQT^{4+}$ ring has localized on the oxyphenylene stations upon formation of the TTF^{2+} dication. Similar observations (Figure 2d−f) were made for rotaxanes $\mathbf{R}_M^{4+}$, $\mathbf{R}_L^{4+}$, and $\mathbf{R}_{XL}^{4+}$ following oxidation and switching.

Location of the Ring in the Switched States $\mathbf{SR}^{6+}$ and $\mathbf{SR}^{4+}$ as a Function of Linker Length. While switching is clearly evident from the ^{1}H NMR spectra of all oxidized species, differences in the chemical shift positions of the protons associated with the oxyphenylene station and neighboring glycolic protons indicate that the $CBPQT^{4+}$ ring is centralized on the oxyphenylene station to differing degrees across the switched rotaxanes (Figure 2c−f). Among the rotaxanes, the one with the shortest linker, $\mathbf{SR}_S^{6+}$ (Figure 2c), shows the largest effect of shielding on the oxyphenylene protons concomitant with the smallest shielding on the neighboring glycolic chain. These observations indicate that the ring is closer to the oxyphenylene station in the short rotaxane. In the extra long rotaxane, $\mathbf{SR}_{XL}^{6+}$ (Figure 2f), however, greater shielding effects are seen on the glycolic chain, while the oxyphenylene protons are less shielded than in the short rotaxane $\mathbf{SR}_S^{6+}$. Thus, the $CBPQT^{4+}$ ring spends more of its time surrounding the oxyphenylene protons when the linker is short. Consistently, NMR data of the rotaxanes with the medium and long linkers show chemical shifts that are positioned between the two extremes.

The preference of the $CBPQT^{4+}$ ring for the oxyphenylene unit in $\mathbf{SR}_S^{6+}$ when compared to the longer rotaxanes $\mathbf{SR}_L^{6+}$ and $\mathbf{SR}_{XL}^{6+}$ could arise from stronger electrostatic repulsions between the dicationic TTF^{2+} and the tetracationic $CBPQT^{4+}$ ring on account of the shorter distance between like charges. In order to investigate this hypothesis, a set of rotaxanes (Figure 3a) was designed to serve as controls in which the thioether is changed from SMe to a larger SEt.

It is known[25] that the electrostatic repulsion provided by an oxidized TTF^{2+} provides additional impetus for the tetracationic $CBPQT^{4+}$ to pass over the SEt speed bump to prepare SEt−$\mathbf{SR}^{6+}$ (see Figures S5 and S6). However, the SEt barrier is too big for

dx.doi.org/10.1021/ja5013596 | *J. Am. Chem. Soc.* 2014, 136, 6373−6384

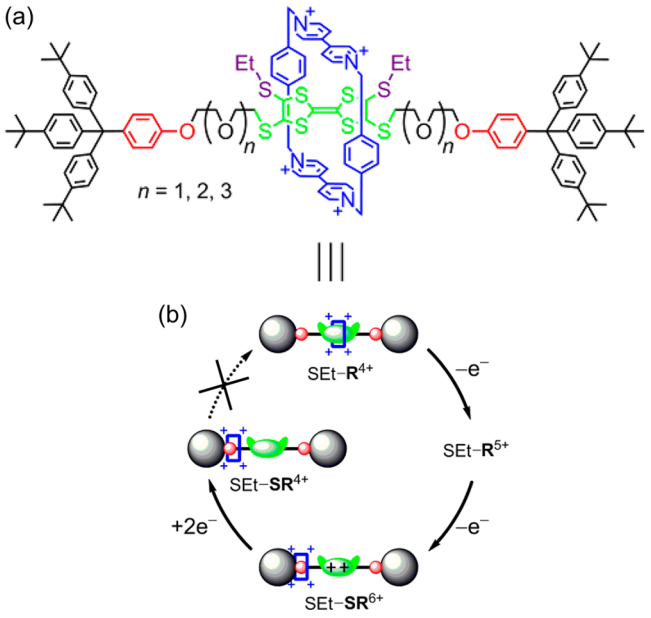

Figure 3. (a) Molecular structure describing [2]rotaxane SEt–$\mathbf{R_S}^{4+}$ (n = 1), SEt–$\mathbf{R_M}^{4+}$ (n = 2), and SEt–$\mathbf{R_L}^{4+}$ (n = 3). (b) Generalized cartoon representations illustrating the preparation of SEt–$\mathbf{SR}^{4+}$ starting from SEt–$\mathbf{R}^{4+}$.

the CBPQT^{4+} ring to return again after reduction to the neutral TTF unit, and consequently, SEt–$\mathbf{SR_S}^{4+}$ is produced (Figure 3b). These control rotaxanes allow us to test if the tetracationic CBPQT^{4+} ring alters its position in the switched state when the neutral TTF unit is present (e.g., SEt–$\mathbf{SR}^{4+}$) and therefore represents the situation when electrostatic repulsions from TTF^{2+} dication can be excluded. The rotaxanes were synthesized in a similar fashion to the title compounds (see Supporting Information).[53]

The ^{1}H NMR spectrum (Figure 4) of the oxidized SEt-based rotaxane with the short linker (SEt–$\mathbf{SR_S}^{6+}$) shows features consistent with linear translation of the CBPQT^{4+} ring to one of the O-linked oxyphenylene stations. This fact is made obvious from the ^{1}H NMR spectrum (Figure 4b), which is almost identical to the one observed for the similar SMe-based rotaxane ($\mathbf{SR_S}^{6+}$, Figure 4c). The only exception lies with the SMe signals now being replaced by resonances from the SEt groups (Figure 4b). After reduction using Zn powder, the neutral rotaxane SEt–$\mathbf{SR_S}^{4+}$ is produced. The resulting ^{1}H NMR spectrum (Figure 4d) has a greater similarity to the spectrum of the oxidized rotaxane SEt–$\mathbf{SR_S}^{6+}$ (Figure 4b) than it has to its parent rotaxane SEt–$\mathbf{R_S}^{4+}$ (Figure 4a) present at the beginning. For instance, the chemical shift position (Figure 4d) of the oxyphenylene protons H_a (δ = 6.25 ppm) and H_b (δ = 2.53 ppm) and the two methylene groups (–O–CH_2–CH_2–) at ca. 3.5 and 1.5 ppm attached directly to the encircled oxyphenylene station in SEt–$\mathbf{SR_S}^{4+}$ almost completely retain their shielded positions (Figure 4d). The hydrogen resonances on the –O–CH_2–CH_2– linker attached directly to the oxyphenylene station move slightly more upfield (Figure 4d) in SEt–$\mathbf{R_S}^{4+}$ than either of the oxidized rotaxanes. We attribute this observation to the proximity of the neutralized TTF rather than any movement of the CBPQT^{4+} ring toward the –O–CH_2–CH_2– group. The SEt–based rotaxanes with medium and long linkers show identical outcomes. These observations are consistent with electrostatics only playing a small role in positioning CBPQT^{4+} in the oxidized, switched rotaxanes.

Returning to the fact that the CBPQT^{4+} appears to remain on the oxyphenylene station in the SEt-based rotaxanes after the TTF unit is returned to its neutral form suggests that the CBPQT^{4+} ring could have some small affinity for the oxyphenylene station. This idea is consistent with the fact that the oxyphenylene's H_b protons seem to be engaged in C–H···π interactions with the CBPQT^{4+} ring (vide supra) and can also be explained by the chemical similarity between an oxyphenylene unit and a hydroquinone (HQ) moiety, which is known[54] to act as a station for CBPQT^{4+}. A binding study between CBPQT^{4+} and the bulky stopper unit bearing the long glycol linker (see Scheme S2 and Figure S7) was conducted. The free energy obtained ΔG° = –1.65 kcal mol^{-1} (K_a = 16 M^{-1}) for the complexation in CD_3CN at 298 K confirms that CBPQT^{4+} binds a little to the oxyphenylene unit, and this finding could explain the CBPQT^{4+} ring's positioning in the switched rotaxanes.

Mechanistic Studies of the Switching Reactions Using CV. Electrochemistry has been widely used to study switching processes in mechanically interlocked systems.[27,34,55–57] In

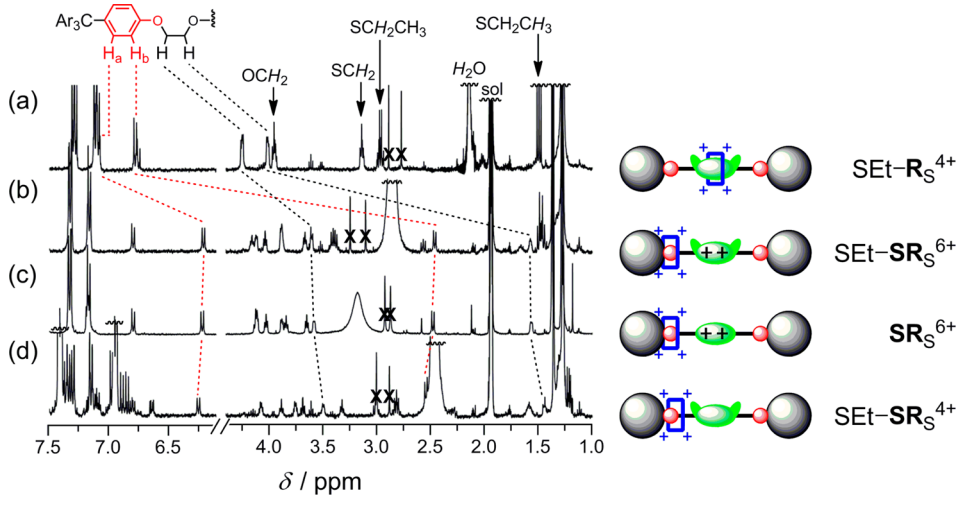

Figure 4. Partial ^{1}H NMR spectra (400 MHz, 298 K, CD_3CN, 2.0 mM) of (a) SEt–$\mathbf{R_S}^{4+}$, (b) SEt–$\mathbf{SR_S}^{6+}$, (c) $\mathbf{SR_S}^{6+}$, and (d) SEt–$\mathbf{SR_S}^{4+}$. The switched rotaxanes (SEt–$\mathbf{SR_S}^{6+}$ and $\mathbf{SR_S}^{6+}$) are generated by adding 10 equiv of the oxidant $TBPASbCl_6$. SEt–$\mathbf{SR_S}^{4+}$ is generated by adding Zn powder to SEt–$\mathbf{SR_S}^{6+}$. The signals being crossed out arise from traces of DMF present in the samples after the synthesis.

dx.doi.org/10.1021/ja5013596 | J. Am. Chem. Soc. 2014, 136, 6373–6384

particular, CV is an electrochemical method that allows for the addition and removal of electrons by applying specific potentials to the working electrode. Current peaks (I_p) in the CV response at specific voltages (V) correspond to oxidation and reduction events. All peak positions for anodic oxidations and cathodic reductions, E_{pa} and E_{pc}, respectively, will be distinguished as peaks, and all half wave potentials, (i.e., $E_{1/2} = (E_{pa} + E_{pc})/2$) will be called waves. Some of the oxidation events that are observed in the forward sweep (0 → +1 V versus Ag/AgCl) also serve as triggers to stimulate translational movements in bistable rotaxanes, while the reduction peaks during the return sweep (+1 → 0 V) remove the stimulus. The time between addition and removal of the stimulus is available for the ring's movement. Changing the sweep rate of the CV can easily vary this time period. The extent of molecular switching can then be analyzed by using the return CV sweep on account of the fact that peak heights, I_p, are proportional to concentration according to the Randles–Sevcik relation.[58] For this reason, the return sweeps are often used to analyze the products of redox-driven switching.

The redox responses of the dumbbells were studied as controls. The short dumbbell, $\mathbf{D}_S$ (for its structure, see Scheme S1), showed two redox waves ($E_{1/2}$, as above) at +0.46 and +0.75 V (Figure 5a) corresponding to the first and second oxidation of TTF, respectively, which is consistent with previous studies.[18]

The redox potentials of both the initial and switched forms of each rotaxane, e.g., $\mathbf{R}^{4+}$ and $\mathbf{SR}^{6+}$, were measured by utilizing fast scan rates (>10 V s^{-1}) in order to minimize any switching. Under these conditions, each rotaxane had similar redox potentials (Table 1) irrespective of the linker's length. Variable scan rates were used to temporally resolve the switching speeds. Each of the CV responses show that all the rotaxanes follow the same well documented mechanism of switching according to the sequence, oxidation-move-oxidation (ox-move-ox, Scheme 1) for the forward switching from $\mathbf{R}^{4+}$ to $\mathbf{SR}^{6+}$. The redox response of the short rotaxane $\mathbf{R}_S^{4+}$ is described in depth and is representative of the features seen with all four rotaxanes

Switching Rates in the Short Rotaxane—Escape in the Forward Direction. Rotaxane $\mathbf{R}_S^{4+}$ displayed a one-electron oxidation peak in the forward scan of the CV at +0.86 V (Figure 5b, red trace), which is ∼400 mV more positive than the first oxidation of the dumbbell $\mathbf{D}_S$. This observation is consistent with prior studies[18,59] and follows from the fact that more energy is required to oxidize the TTF unit when it is encircled by the tetracationic ring. Scanning further out to ∼+1.4 V at fast scan rates (10 V s^{-1}) and at 273 K reveals (Figure S12) the second oxidation of the rotaxane $\mathbf{R}_S^{5+}$ to $\mathbf{R}_S^{6+}$ that occurs prior to the ring's movement away from the monocationic TTF^+ unit. In a separate experiment, holding the potential above +1 V for a sufficient period of time (10 s) ensures generation of the switched rotaxane, $\mathbf{SR}^{6+}$, at the electrode surface within the diffusion layer. Performing a fast sweep back to 0 V allows the redox potentials of the switched rotaxane to be identified (Figure 5c, red trace). The switched rotaxane shows two redox waves in this forward sweep at +0.42 and +0.65 V that have very similar potentials to the redox waves of the free dumbbell (Figure 5a), indicating the $CBPQT^{4+}$ ring no longer encircles the TTF unit. These data are in line with the interpretations from the chemical oxidation studies described above.

To characterize the kinetics of the forward switching reaction, the potential was swept from 0 to +1.1 V and back again using different scan rates (Figure 5b). Slower scan rates allow more time for the rotaxanes to switch. Starting from 10 V s^{-1} (red trace, Figure 5b) and slowing down the scan rate, the initial one-

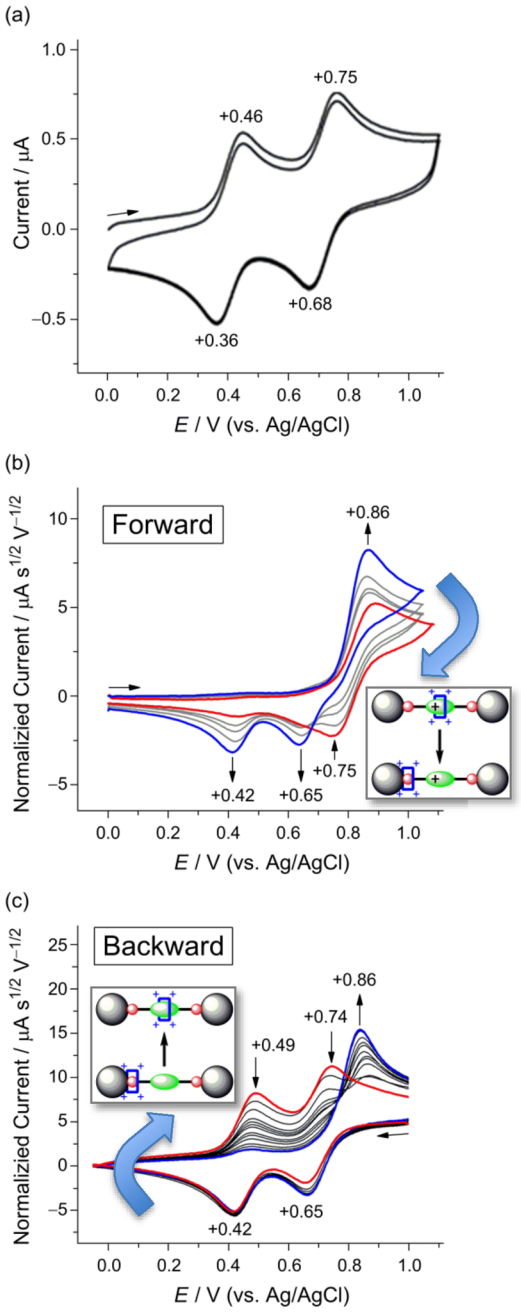

Figure 5. Representative CVs illustrating that motion occurs by comparing the (a) dumbbell $\mathbf{D}_S$ (0.25 mM, 0.1 M $TBAPF_6$, 2:1 CH_2Cl_2:MeCN, CH_2Cl_2 added for solubility), (b) rotaxane $\mathbf{R}_S^{4+}$ (2 mM, 0.1 M $TBAPF_6$, MeCN, 273 K) starting with $\mathbf{R}^{4+}$ showing changes in relative peak positions (arrows) with decreasing scan rate (red trace: 10 V s^{-1} – blue trace: 0.2 V s^{-1}), and (c) rotaxane $\mathbf{R}_S^{4+}$ (2 mM, 0.1 M $TBAPF_6$, MeCN, 298 K) starting with the switched rotaxane $\mathbf{SR}^{6+}$ showing changes in relative peak positions (arrows) with decreasing scan rate (red: 10 V s^{-1} – blue: 0.25 V s^{-1}). Glassy carbon working electrode.

electron peak in the forward sweep at +0.86 V is observed to increase in magnitude as the second oxidation takes place. These increases arise from the ox-move-ox sequence (Scheme 1). First, $\mathbf{R}_S^{4+}$ is oxidized by one electron to $\mathbf{R}_S^{5+}$, which initiates the ring's movement to the oxyphenylene station, generating $\mathbf{SR}_S^{5+}$. After the $CBPQT^{4+}$ ring has moved, the potential at the working electrode provides a thermodynamically favored environment to

dx.doi.org/10.1021/ja5013596 | J. Am. Chem. Soc. 2014, 136, 6373–6384

Table 1. Electrochemical Data[a] for the Initial and Switched Rotaxanes

	$E_{1/2}$ [V]				E_{pa} [V]			
	SR_S^{4+}	SR_M^{4+}	SR_L^{4+}	SR_{XL}^{4+}	R_S^{4+}	R_M^{4+}	R_L^{4+}	R_{XL}^{4+}
Ox1	+0.48	+0.47	+0.45	+0.49	+0.86[b]	+0.84[b]	+0.83[b]	+0.80[b]
Ox2	+0.71	+0.70	+0.68	+0.71				

[a]Conditions for the CV: 0.1 M $TBAPF_6$, MeCN, c = 2.0 mM, glassy carbon working electrode, Pt counter electrode, scan rate >10 V s^{-1}, $E_{1/2}$ and E_{pa} values vs Ag/AgCl, errors ±0.01 V. [b]Anodic oxidation peak.

immediately oxidize SR_S^{5+} to SR_S^{6+}. During the subsequent analysis sweeps (from +1.1 to 0 V), the temporal resolution of the movement away from the TTF^+ in the ox-move-ox sequence is also made obvious. The peak at +0.75 V, which is assigned to the reduction of the unswitched rotaxane R_S^{5+} (red trace, Figure 5b), is most intense using faster scan rates and is then observed to decrease in size as the scan rate slows down. Concomitantly, the switched rotaxane, SR_S^{6+}, is formed, and its associated peaks at +0.65 and +0.42 V (blue trace, Figure 5b) that correspond to sequential reduction of SR_S^{6+} and SR_S^{5+}, are observed to increase in intensity. The voltage window scanned from the initial oxidation at +0.86 V out to the return voltage (+1.1 V) and back to the first reduction at ∼+0.7 V amounts to a 0.65 V span, which can give rise to a 65 ms (10 V s^{-1}) to 3.25 s (0.2 V s^{-1}) time window to resolve the escape motion associated with $R_S^{5+} \rightarrow SR_S^{5+}$.

Switching Rates in the Short Rotaxane: Return Movement. The return switching can be characterized in a similar manner (Figure 5c). Initially, the potential is held above +1 V for 10 s to generate SR_S^{6+} in the diffusion layer, and thereafter, the potential is swept to 0 V and back again at various scan rates. Upon scanning from +1 to 0 V, reduction to SR_S^{4+} takes place at +0.42 V. After it is generated, $CBPQT^{4+}$ moves to the neutral TTF to generate R_S^{4+} such that the return sweep in the CV (0 → +1 V) represents a reduction-reduction-move sequence (Scheme 1). During this sweep the relative amounts of the metastable switched rotaxane SR_S^{4+} and the product rotaxane R_S^{4+} can be analyzed to capture the departure and arrival of the ring. Slow scan rates (blue trace, Figure 5c) allow R_S^{4+} to be fully formed. At fast scan rates, SR_S^{4+} is still present in the diffusion layer. This metastable species can be identified from the peak at +0.49 V (red trace, Figure 5c), which has a very similar potential to the oxidation peak for the dumbbell (Figure 5a) indicating that the TTF unit is still unencircled. Based on the voltage window scanned, a time window of 90 ms (10 V s^{-1}) to 3.6 s (0.25 V s^{-1}) was available for resolving the return movement, $SR_S^{4+} \rightarrow R_S^{4+}$, of the ring from the oxyphenylene to the TTF station.

Rates of Motion as a Function of Linker Length. The overall sequence for switching forward and backward (Scheme 1) was used as a basis to simulate and reproduce the shapes of the CVs recorded at different scan rates (see Figures S13–S24). Close correlations between the simulated and experimental data enabled the kinetics parameters for each of the molecular movements to be determined. The observed rate of escape (k_{293}^{obs}) in the forward direction toward the oxyphenylene stations has two equal probability pathways, to the left and to the right. Consequently, the observed rate constants were halved (k) in order to provide estimates of the microscopic activation parameters ($\Delta G^{\ddagger}$, $\Delta H^{\ddagger}$, $\Delta S^{\ddagger}$) associated with overcoming just one barrier at a time.

The four different rotaxanes displayed similar $E_{1/2}$ values (Table 1), indicating that the linkers do not have an effect on their thermodynamics. CVs of three of the rotaxanes (R_S^{4+}, R_M^{4+}, and R_L^{4+}) could be readily simulated using the same electrochemical switching sequence (Scheme 1 and Supporting Information). The rate constants (Table 2) for the movement of the $CBPQT^{4+}$ ring away from the TTF^+ unit ($R^{5+} \rightarrow SR^{5+}$) were optimized to fit the scan-rate-dependent shapes of the CVs; compare experimental and simulated CVs in Figure S13. Surprisingly, when the linker was doubled in length, R_S^{4+} and R_L^{4+}, the time taken for the $CBPQT^{4+}$ ring to escape from the TTF^+ monocation over the barrier did not increase but instead decreased by a factor of 3 with $t_{1/2}$ = 60 and 21 ms, respectively. This result is in contrast with previous studies[26,37] where longer linkers slowed the overall rates of reaction. The CV data recorded on the rotaxane with extra long ethylene glycol linkers (R_{XL}^{4+}) are consistent with the same sequence of steps, however, the rates of switching were outside the range of the present experimental setup. The return switching reaction (Table 3) showed longer linkers slowing the movements more dramatically from $t_{1/2}$ = 1.4 to 17 s (293 K); a factor of 10 or more when the linker's length is doubled.

Escape in the Forward Direction: Activation Enthalpy and Entropy. Motivated by the unexpected rate enhancement seen for escape in the forward direction, variable-temperature studies of the three rotaxanes (R_S^{4+}, R_M^{4+}, and R_L^{4+}) were conducted to determine the activation parameters in a bid to shed light on the nature of the RLS. Variable-temperature data (263−303 K) for the forward switching was used in an Eyring analysis (Figure 6a). Even though the rates of the forward reaction across the three rotaxanes (R_S^{4+}, R_M^{4+}, and R_L^{4+}) increased with the linker's length, the least-squares regression of the Eyring plots produced activation parameters ($\Delta H^{\ddagger}$, $\Delta S^{\ddagger}$) that were the same to within error (Table 2) and dominated by an enthalpy barrier we attribute to sterics.

The negative activation entropies of approximately −4 cal K^{-1} mol^{-1}, suggest there is a modest increase in the ordering of the transition state structure in $R^{5+\ddagger}$ relative to the initial structure of R^{5+}. The fact that this ordering is so small is consistent with an early transition state. The structure proposed for the intermediate state R_S^{5+} (Scheme 2) is based on the idea that electrostatic repulsions from the monocationic TTF^+ unit repel the tetracationic $CBPQT^{4+}$ ring. Consequently, the $CBPQT^{4+}$ ring is expected to move toward the neutral half of the TTF^+ unit where it is forced up against the SMe and $-S-CH_2-CH_2-O-$ chains, which together act as steric blocking groups. In this situation, with $CBPQT^{4+}$ abutted against the steric barrier, it is conceivable that the two chains might already be preorganized in a favorable manner to help mitigate the entropic contribution to the barrier, see the RLS in Scheme 2 for models of the intermediate, R_S^{5+}, and the transition state, $R_S^{5+\ddagger}$.

The fact that all three rotaxanes (R_S^{4+}, R_M^{4+}, and R_L^{4+}, Table 2) show similar sets of activation parameters ($\Delta G^{\ddagger}$ ∼ +15 kcal mol^{-1}, $\Delta H^{\ddagger}$ ∼ +14 kcal mol^{-1}, $\Delta S^{\ddagger}$ ∼ −4 cal K^{-1} mol^{-1}) indicates that the RLSs to escape have shared qualities. Nevertheless, there is a measurable impact of the linker's length on the rate constants of escape indicating their involvement. This effect was enhanced further with the extra long rotaxane (R_{XL}^{4+}),

dx.doi.org/10.1021/ja5013596 | J. Am. Chem. Soc. 2014, 136, 6373−6384

Table 2. Kinetics and Associated Activation Parameters for the Forward Movement ($R^{5+} \rightarrow SR^{5+}$) of the CBPQT^{4+} Ring From TTF^{+} Over the SMe Barrier to the Oxyphenylene Station[a,b,c]

	k_{293}^{obs} [s^{-1}]	k_{293} [s^{-1}]	$t_{1/2}$ [ms]	$\Delta G_{293}^{\ddagger}$ [kcal mol^{-1}]	$\Delta H^{\ddagger}$ [kcal mol^{-1}]	$\Delta S^{\ddagger}$ [cal K^{-1} mol^{-1}]
short	23 ± 1.2	11.5 ± 1.2	60	15.7 ± 0.1	14.5 ± 1.0	−4.1 ± 3.6
medium	40 ± 2	20 ± 2	35	15.4 ± 0.1	13.8 ± 0.5	−5.5 ± 1.6
long	65 ± 3.5	32.5 ± 3.5	21	15.2 ± 0.1	14.5 ± 0.5	−2.3 ± 1.8
extra long	>200	>100	<7	>14.5		

[a]Conditions for the CV: 0.1 M $TBAPF_6$, MeCN, 2.0 mM, glassy carbon working electrode, Pt counter electrode, 263−303 K, 10−0.2 V s^{-1}. [b]k_{293}^{obs} is the observed rate of escape from the TTF^{+} station over either barrier; k_{293}, $t_{1/2}$, $\Delta G_{293}^{\ddagger}$, $\Delta H^{\ddagger}$, and $\Delta S^{\ddagger}$ are the values for microscopic activation parameters. [c]Values for k_{293} and $t_{1/2}$ are determined as follows: $k_{293} = 0.5\ k_{293}^{obs}$ and $t_{1/2} = \ln(2) k_{293}^{-1}$.

Table 3. Kinetics and Associated Activation Parameters for the Return Movement ($SR^{4+} \rightarrow R^{4+}$) of the CBPQT^{4+} Ring from the Oxyphenylene Station Back Over the SMe Barrier to the TTF Station[a]

	k_{293} [s^{-1}]	$t_{1/2}$ [s]	$\Delta G_{293}^{\ddagger}$ [kcal mol^{-1}]	$\Delta H^{\ddagger}$ [kcal mol^{-1}]	$\Delta S^{\ddagger}$ [cal K^{-1} mol^{-1}]
short	0.50 ± 0.08	1.4	17.6 ± 0.1	6.9 ± 0.9	−37 ± 3
medium	0.10 ± 0.03	6.9	18.5 ± 0.2	12 ± 1	−20 ± 2
long	0.04 ± 0.01	17.3	19.0 ± 0.2	17 ± 1	−6.6 ± 2.5
extra long	<0.01	>69	>19.8		

[a]Conditions for the CV: 0.1 M $TBAPF_6$, MeCN, 2.0 mM, glassy carbon working electrode, Pt counter electrode, 293−333 K, 10−0.2 V s^{-1}.

which takes <7 ms, confirming the veracity of this trend. The most likely explanation for the increased rates for the forward reaction is the increasing involvement of the longer glycolic linkers in stabilizing the CBPQT^{4+} ring[41] when it passes over the sterically-based transition state ($R_L^{5+\ddagger}$, Scheme 3).

After passing over the steric barrier, the CBPQT^{4+} ring moves to the oxyphenylene station at speeds that cannot be distinguished using this current series of rotaxanes. This idea is consistent with Leigh's study[23] that RLSs in interlocked molecules tend to be dominated by escape from the initial station. Removal of the SMe groups might shift the RLS to be one that depends on the ring's movement along the linker. Furthermore, use of a secondary station that is redox-active would allow the time of the ring's arrival to be measured.

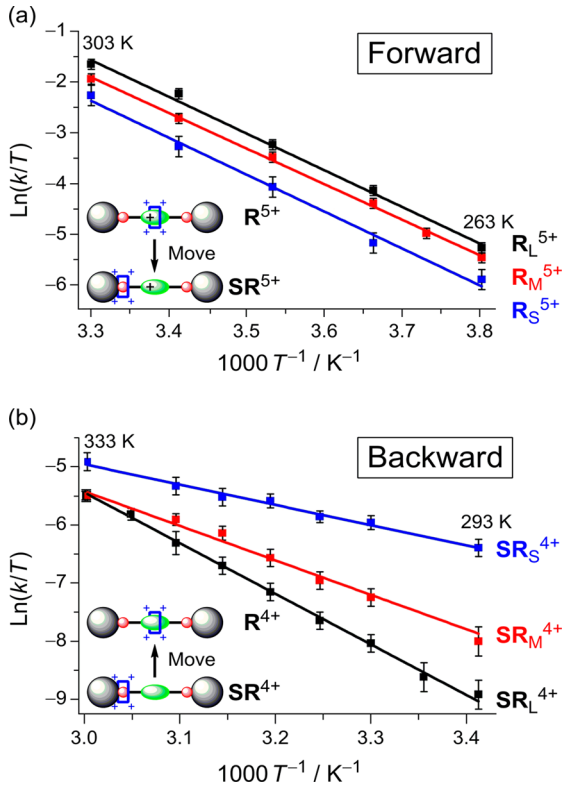

Figure 6. Eying plots for the (a) forward and (b) reverse movement of CBPQT^{4+} along rotaxanes R_S^{4+}, R_M^{4+}, and R_L^{4+} as determined using kinetic parameters from the CV simulations.

Return Switching and Intermediates on Pathway Between Stations. An Eyring analysis of the return switching (Figure 6b, 293−333 K), for which the departure and arrival times are measured, shows that longer linkers slow the rate (Table 3) of motion considerably and that the nature of the RLS also changes. The movement of the CBPQT^{4+} ring from the oxyphenylene station back to the neutral TTF unit in the rotaxane with a short linker ($t_{1/2}$ = 1.4 s, $\Delta G^{\ddagger}$ = +17.6 kcal mol^{-1}) has a small enthalpy of activation, $\Delta H^{\ddagger}$ = +6.9 ± 0.9 kcal mol^{-1}, while the activation entropy is large and negative, $\Delta S^{\ddagger}$ = −37 ± 3 cal K^{-1} mol^{-1}. The magnitude of this entropic factor is consistent with the need for a significant increase in the ordering of both the SMe thioether and the glycol linker to allow passage of the CBPQT^{4+} ring ($SR_S^{4+\ddagger}$, Scheme 2).

By contrast, the long rotaxane shows a barrier ($t_{1/2}$ = 17.3 s, $\Delta G^{\ddagger}$ = +19 kcal mol^{-1}) that is now enthalpic in nature ($\Delta H^{\ddagger}$ = +17 ± 1 kcal mol^{-1}) with a much-reduced entropic contribution ($\Delta S^{\ddagger}$ = −6.6 ± 2.5 cal K^{-1} mol^{-1}). The large activation enthalpy supports the idea that the longer rotaxane needs to break additional stabilizing interactions between the CBPQT^{4+} ring and glycol chain before moving over the steric barrier. The fact that glycol chains can bind to CBPQT^{4+} is confirmed in the literature[40,41,60] and is typically observed as CH···O hydrogen-bond interactions between the α-CH hydrogens atoms in the bipyridinium units of CBPQT^{4+} and the oxygen atoms present in the glycol chains. If the interactions are in fact present as CH···O hydrogen bonds, they are likely to be highly ordered (Scheme 3, $SR_L^{4+\ddagger}$). Therefore, breaking these contacts should be an entropically favorable process, as the glycols would then be free to move. The configurational entropy is associated with increased freedom of the glycol chains on going from the small to medium (13 cal K^{-1} mol^{-1}) and small to long rotaxanes (30 cal K^{-1} mol^{-1}), corresponding to extensions by ethylene and diethylene glycol, respectively. These values are consistent with the loss in entropy (~6 cal K^{-1} mol^{-1}, Me_2CO) observed for the

dx.doi.org/10.1021/ja5013596 | J. Am. Chem. Soc. 2014, 136, 6373−6384

Scheme 2. Proposed Mechanism for the Switching Cycle in the Short Rotaxane R_S^{4+}[a]

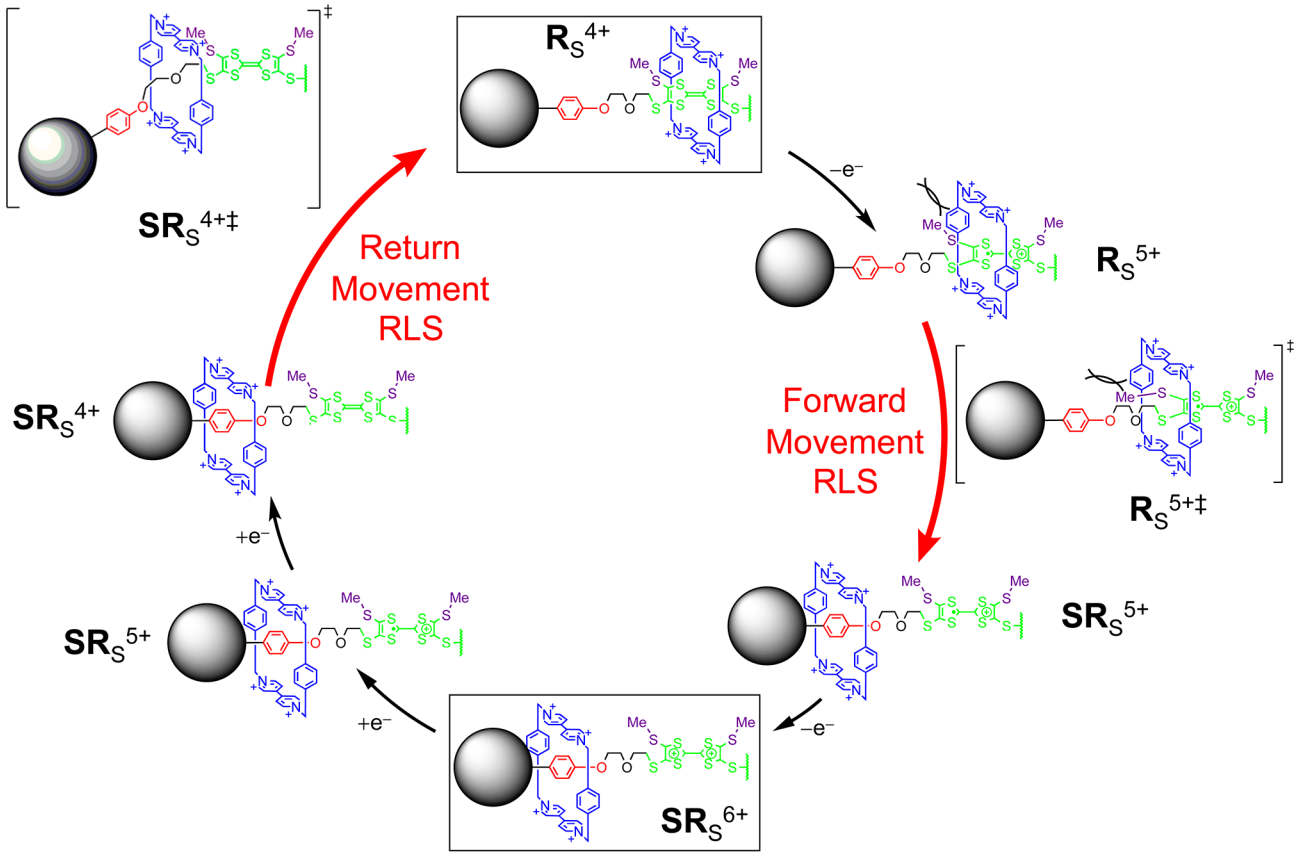

[a]The RLS is indicated for both the forward and return directions of motion.[65]

binding of $CBPQT^{4+}$ to monopyrrolo-TTF when a triethylene glycol unit was wrapped around the bipyridinium.[41]

The structure of the switched rotaxane $\mathbf{SR_L}^{4+}$ (Scheme 4) would likely involve a folded conformation where the neutral TTF unit is contacting one side of the $CBPQT^{4+}$ ring to form a weak charge-transfer interaction, which would also impact the $\Delta H^{‡}$ and $\Delta S^{‡}$. Evidence for these alongside effects is growing in the literature.[61−64] The movement of the $CBPQT^{4+}$ ring from the oxyphenylene back to the neutral TTF unit is too fast to isolate $\mathbf{SR_L}^{4+}$ for analysis, consequently, evidence for the alongside interaction was achieved using the switched form of the blocked long rotaxane SEt−$\mathbf{SR_L}^{4+}$ (Figure 3). Starting from SEt−$\mathbf{R_L}^{4+}$, oxidation followed by reduction, purification, and ion exchange (see Supporting Information) afforded a sample for analysis. A UV−vis−NIR spectrum of SEt−$\mathbf{SR_L}^{4+}$ (MeCN, 280 K, Figure 7) was measured, and a weak charge-transfer absorption was located at 625 nm[64] that would be expected from a folded conformation (Scheme 4). We believe this structure will also be present in the metastable intermediate $\mathbf{SR_L}^{4+}$ prior to movement of the $CBPQT^{4+}$ ring back to TTF station.

The presence of a folded structure in $\mathbf{SR_L}^{4+}$ requires the charge-transfer interactions between the TTF group and the $CBPQT^{4+}$ ring to be broken before it is free to move (Scheme 3). Furthermore, it is known from the binding study (*vide supra*) that there is a stable interaction between the $CBPQT^{4+}$ ring and the oxyphenylene station, which may be governed by C−H···π interactions between the encircled oxyphenylene's protons and the *p*-xylyl rings of $CBPQT^{4+}$ as was shown in the ^{1}H NMR spectra (Figure 2). All of these noncovalent interactions have to be broken in order for the $CBPQT^{4+}$ to move, and they all contribute to the large enthalpic barrier. The unfolding of the structure to allow movement of the $CBPQT^{4+}$ ring would also be entropically favorable. The same folded structure must be present in the extra long rotaxane to account for the fact that its switching is even slower. In the shortest rotaxane $\mathbf{SR_S}^{4+}$ (Scheme 2), it has fewer CH···O hydrogen bonds and is less competent at forming the alongside charge-transfer interactions; consequently, it has less bonds to break and has less entropy offset during its switching back to $\mathbf{R_S}^{4+}$.

Impacts of Linker Length on Time-Resolved Movements Forward and Backward. In summary (Figure 8), the escape from the primary station gets faster with longer linkers, while the return movement from the secondary to the primary station slows down. Prior to initiating the return movement, the switched rotaxane with the long linker, $\mathbf{SR_L}^{4+}$, has the possibility to fold up into a more compact and thermodynamically stable structure by making noncovalent interactions (Scheme 3). These contacts contribute to the high enthalpy ($\Delta H^{‡}$) barrier of activation and the freedom gained upon unfolding leads to a smaller entropic ($\Delta S^{‡}$) barrier in the reverse switching of the long rotaxane, $\mathbf{R_L}^{4+}$. Conversely the short rotaxane, $\mathbf{R_S}^{4+}$ has a high entropy ($\Delta S^{‡}$) factor because the increased ordering in the substituent (the SMe thioether and the short glycol linker) that is required for $CBPQT^{4+}$ to move back to the neutral TTF (Scheme 2) is not offset as it is with $\mathbf{R_L}^{4+}$. Across the series, the linker's length has a minor effect on the forward escape and a large impact on the return movement. For the short rotaxane, the forward and return movements shunt the ring between stations. Whereas, the extra long rotaxane's movements reflect a shove

dx.doi.org/10.1021/ja5013596 | J. Am. Chem. Soc. 2014, 136, 6373−6384

Scheme 3. Proposed Mechanism for the Switching Cycle in the Long Rotaxane R_L^{4+} [a]

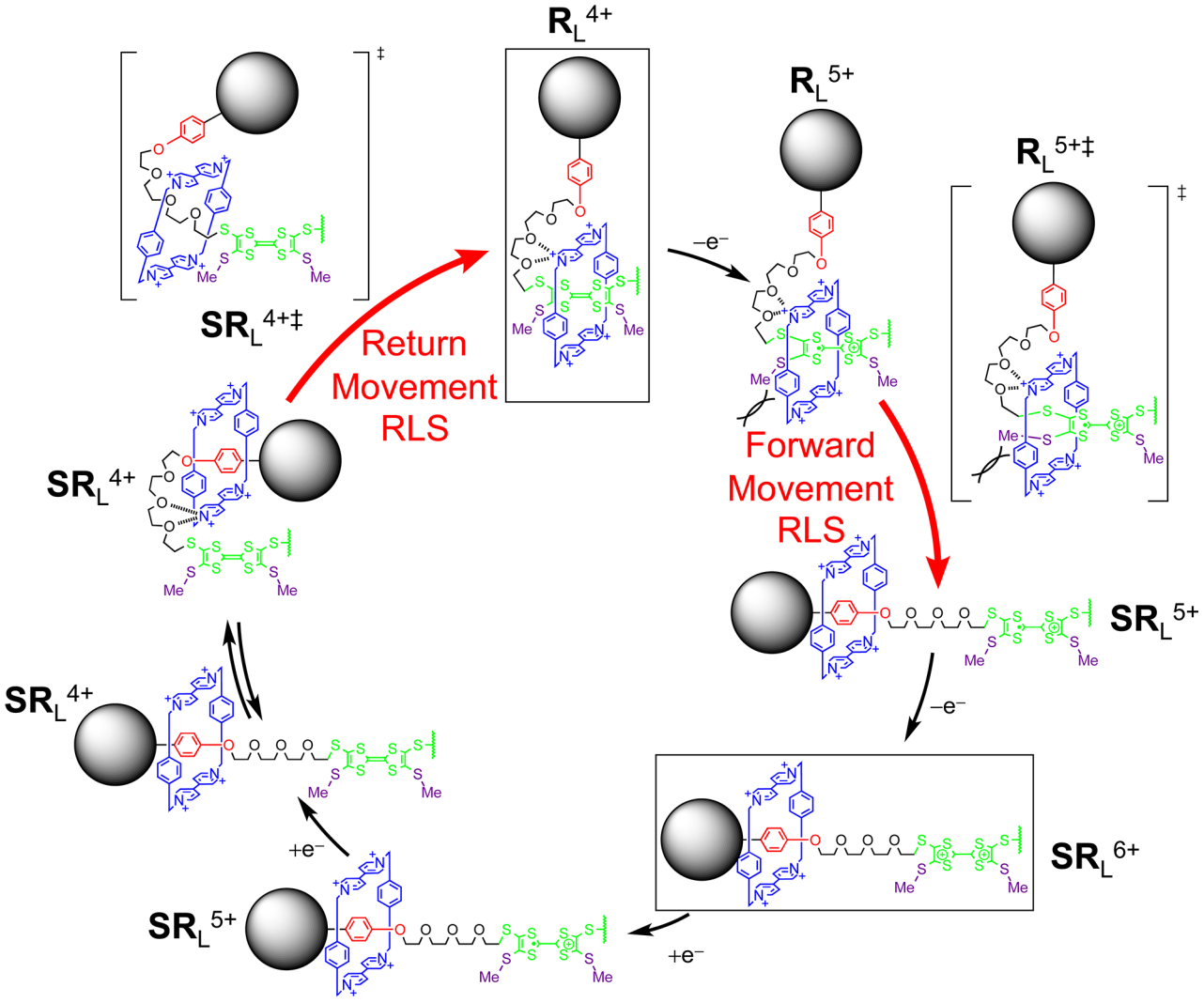

[a]The RLS is indicated for both the forward and return directions of motion.[65]

Scheme 4. Equilibrium Between the Folded and Unfolded Structure of SEt–SR_L^{4+} [a]

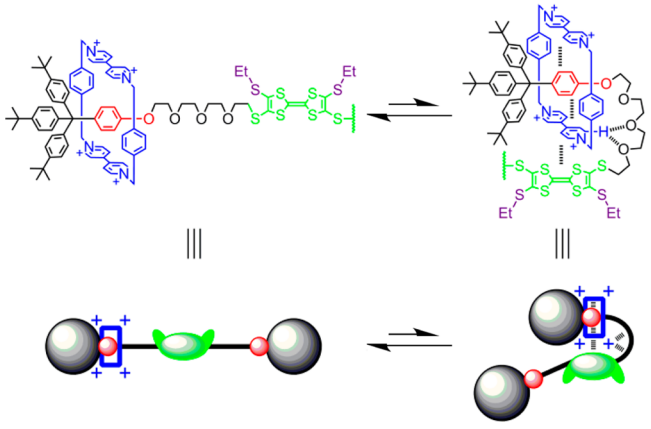

[a]The structure shows the possibility of forming CH···O and charge-transfer interactions in the folded alongside conformation (right) that brings the oxyphenylene-localized $CBPQT^{4+}$ into contact with the neutral TTF unit.

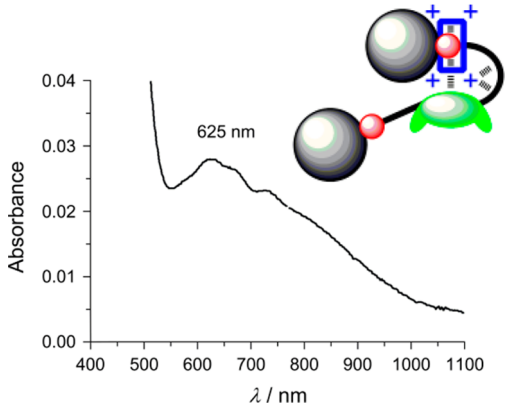

Figure 7. UV–vis–NIR absorption spectrum of SEt–SR_L^{4+} recorded in MeCN (0.2 mM) at 280 K.

over the steric barrier to access the secondary station and generate a folded coconformation that, after reduction to the neutral TTF unit (TTF^0), must unfurl at some point during passage of the $CBPQT^{4+}$ ring back to the starting point.

dx.doi.org/10.1021/ja5013596 | J. Am. Chem. Soc. 2014, 136, 6373–6384

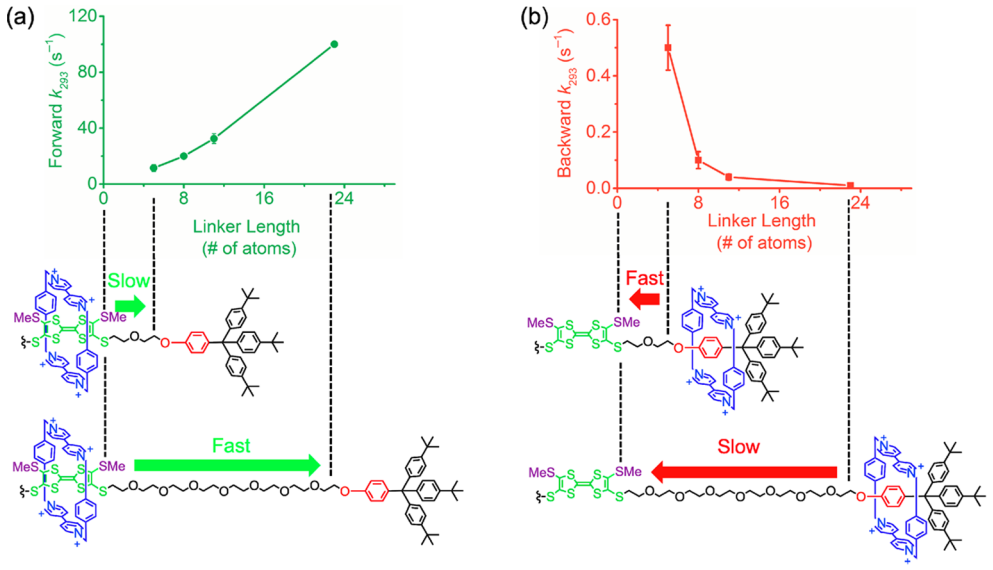

Figure 8. Plots showing how the rate constants of motion change as a function of linker length for (a) escape forward and (b) return movements.

CONCLUSION

In this study of the complete cycle of motion in redox-driven TTF-CBPQT^{4+} rotaxanes, we have shown that the linkers that exist between two stations play a critical role in both the kinetics and the mechanism of motion. In these rotaxanes, the RLS for the forward movement of the CBPQT^{4+} ring involves electrostatic preparation of an intermediate that helps organize passage through an early transition state defined by a steric speed bump (SMe). Subsequently, translation of the ring to the oxyphenylene station occurs but was not measured in these experiments. In the return movement from the oxyphenylene to the charge-neutral TTF, it appears that the RLS is determined by the stability and conformation of the mestastable rotaxane. The rotaxane with the longer glycol linkers is more flexible and thereby allows folding into a compact stable structure in which the neutral TTF unit is located alongside the CBPQT^{4+} ring. Therefore, additional noncovalent interactions have to be broken concomitant with attainment of greater conformational freedom during the movement of the CBPQT^{4+} ring back to the neutral TTF unit. In contrast, the rotaxane with the shorter linker makes fewer noncovalent interactions, and the shorter glycol linker has to dramatically increase its ordering to allow CBPQT^{4+} to pass back to the neutral TTF station. This study shows how the linkers' lengths can impact switching rates in ways that differ from and which complement the insights from Leigh's study; there, escape was fast enough to allow random walks to impact rates of movements, and here, the linkers participated in the thermally activated escape. Overall, these insights contribute design guidance for the generation of machines and motors from the switching progenitors.

ASSOCIATED CONTENT

Supporting Information

Syntheses, chemical switching, binding studies, variable scan rate, and variable-temperature CV data, and their analysis. This material is available free of charge via the Internet at http://pubs.acs.org.

AUTHOR INFORMATION

Corresponding Authors

joj@sdu.dk
aflood@indiana.edu

Notes

The authors declare no competing financial interest.

ACKNOWLEDGMENTS

Support is acknowledged from the Villum Foundation (to J.O.J.), the Danish Natural Science Research Council (FNU, Project 11-106744 to J.O.J.), and the NSF (CHE 0844441 to A.H.F.).

REFERENCES

(1) Kinbara, K.; Aida, T. *Chem. Rev.* **2005**, *105*, 1377.
(2) Coskun, A.; Banaszak, M.; Astumian, R. D.; Stoddart, J. F.; Grzybowski, B. A. *Chem. Soc. Rev.* **2012**, *41*, 19.
(3) Kay, E. R.; Leigh, D. A.; Zerbetto, F. *Angew. Chem., Int. Ed.* **2007**, *46*, 72.
(4) Benson, C. R.; Share, A. I.; Flood, A. H. In *Bioinspiration and Biomimicry in Chemistry*; John Wiley & Sons, Inc.: New York, 2012.
(5) Fahrenbach, A. C.; Bruns, C. J.; Cao, D.; Stoddart, J. F. *Acc. Chem. Res.* **2012**, *45*, 1581.
(6) Jeppesen, J. O.; Perkins, J.; Becher, J.; Stoddart, J. F. *Angew. Chem., Int. Ed.* **2001**, *40*, 1216.
(7) Keaveney, C. M.; Leigh, D. A. *Angew. Chem., Int. Ed.* **2004**, *43*, 1222.
(8) Schmidt, T.; Vögtle, F. *Sci. Spectra* **1999**, 58.
(9) Stoddart, J. F. *Chem. Soc. Rev.* **2009**, *38*, 1802.
(10) Andersen, S. S.; Jensen, M.; Sorensen, A.; Miyazaki, E.; Takimiya, K.; Laursen, B. W.; Flood, A. H.; Jeppesen, J. O. *Chem. Commun.* **2012**, *48*, 5157.
(11) Choi, J. W.; Flood, A. H.; Steuerman, D. W.; Nygaard, S.; Braunschweig, A. B.; Moonen, N. N. P.; Laursen, B. W.; Luo, Y.; DeIonno, E.; Peters, A. J.; Jeppesen, J. O.; Xu, K.; Stoddart, J. F.; Heath, J. R. *Chem.—Eur. J.* **2006**, *12*, 261.
(12) Hamacek, J.; Borkovec, M.; Piguet, C. *Dalton Trans.* **2006**, 1473.
(13) Moonen, N. N. P.; Flood, A.; Fernández, J.; Stoddart, J. F. In *Molecular Machines*; Kelly, T. R., Ed.; Springer: Berlin Heidelberg, 2005; Vol. *262*.
(14) Share, A. I.; Parimal, K.; Flood, A. H. *J. Am. Chem. Soc.* **2010**, *132*, 1665.
(15) Astumian, R. D. *Annu. Rev. Biophys.* **2011**, *40*, 289.
(16) Astumian, R. D. *J. Phys. Condens. Mater.* **2005**, *17*, S3753.

dx.doi.org/10.1021/ja5013596 | *J. Am. Chem. Soc.* 2014, 136, 6373−6384

(17) Serreli, V.; Chin-Fa, L.; Kay, E. R.; Leigh, D. A. *Nature* **2007**, *445*, 523.
(18) Flood, A. H.; Peters, A. J.; Vignon, S. A.; Steuerman, D. W.; Tseng, H.-R.; Kang, S.; Heath, J. R.; Stoddart, J. F. *Chem.—Eur. J.* **2004**, *10*, 6558.
(19) Koumura, N.; Geertsema, E. M.; Gelder, M. B. v.; Meetsma, A.; Feringa, B. L. *J. Am. Chem. Soc.* **2002**, *124*, 5037.
(20) Fletcher, S. P.; Dumur, F.; Pollard, M. M.; Feringa, B. L. *Science* **2005**, *310*, 80.
(21) Leigh, D. A.; Wong, J. K. Y.; Dehez, F.; Zerbetto, F. *Nature* **2003**, *424*, 174.
(22) Hernández, J. V.; Kay, E. R.; Leigh, D. A. *Science* **2004**, *306*, 1532.
(23) Baggerman, J.; Haraszkiewicz, N.; Wiering, P. G.; Fioravanti, G.; Marcaccio, M.; Paolucci, F.; Kay, E. R.; Leigh, D. A.; Brouwer, A. M. *Chem.—Eur. J.* **2013**, *19*, 5566.
(24) Avellini, T.; Li, H.; Coskun, A.; Barin, G.; Trabolsi, A.; Basuray, A. N.; Dey, S. K.; Credi, A.; Silvi, S.; Stoddart, J. F.; Venturi, M. *Angew. Chem., Int. Ed.* **2012**, *51*, 1611.
(25) Nygaard, S.; Laursen, B. W.; Flood, A. H.; Hansen, C. N.; Jeppesen, J. O.; Stoddart, J. F. *Chem. Commun.* **2006**, *2*, 144.
(26) Panman, M. R.; Bodis, P.; Shaw, D. J.; Bakker, B. H.; Newton, A. C.; Kay, E. R.; Brouwer, A. M.; Buma, W. J.; Leigh, D. A.; Woutersen, S. *Science* **2010**, *328*, 1255.
(27) Trabolsi, A.; Fahrenbach, A. C.; Dey, S. K.; Share, A. I.; Friedman, D. C.; Basu, S.; Gasa, T. B.; Khashab, N. M.; Saha, S.; Aprahamian, I.; Khatib, H. A.; Flood, A. H.; Stoddart, J. F. *Chem. Commun.* **2010**, *46*, 871.
(28) Zhang, K. D.; Zhao, X.; Wang, G. T.; Liu, Y.; Zhang, Y.; Lu, H. J.; Jiang, X. K.; Li, Z. T. *Angew. Chem., Int. Ed.* **2011**, *50*, 9866.
(29) Durola, F.; Sauvage, J.-P. *Angew. Chem., Int. Ed.* **2007**, *46*, 3537.
(30) Spruell, J. M.; Paxton, W. F.; Olsen, J.-C.; Benitez, D.; Tkatchouk, E.; Stern, C. L.; Trabolsi, A.; Friedman, D. C.; G, W. A., III; Stoddart, J. F. *J. Am. Chem. Soc.* **2009**, *131*, 11571.
(31) Mobian, P.; Kern, J.-M.; Sauvage, J.-P. *Angew. Chem., Int. Ed.* **2004**, *43*, 2392.
(32) Jeppesen, J. O.; Vignon, S. A.; Stoddart, J. F. *Chem.—Eur. J.* **2003**, *9*, 4611.
(33) Baroncini, M.; Silvi, S.; Venturi, M.; Credi, A. *Chem.—Eur. J.* **2010**, *16*, 11580.
(34) Trabolsi, A.; Khashab, N.; Fahrenbach, A. C.; Friedman, D. C.; Colvin, M. T.; Cotí, K. K.; Benítez, D.; Tkatchouk, E.; Olsen, J.-C.; Belowich, M. E.; Carmielli, R.; Khatib, H. A.; Goddard, W. A.; Wasielewski, M. R.; Stoddart, J. F. *Nat. Chem.* **2010**, *2*, 42.
(35) Hirose, K.; Shiba, Y.; Ishibashi, K.; Doi, Y.; Tobe, Y. *Chem.—Eur. J.* **2008**, *14*, 3427.
(36) Sugino, H.; Kawai, H.; Umehara, T.; Fujiwara, K.; Suzuki, T. *Chem.—Eur. J.* **2012**, *18*, 13722.
(37) Deutman, A. B. C.; Monnereau, C.; Elemans, J. A. A. W.; Ercolani, G.; Nolte, R. J. M.; Rowan, A. E. *Science* **2008**, *322*, 1668.
(38) Li, H.; Zhu, Z.; Fahrenbach, A. C.; Savoie, B. M.; Ke, C.; Barnes, J. C.; Lei, J.; Zhao, Y.-L.; Lilley, L. M.; Marks, T. J.; Ratner, M. A.; Stoddart, J. F. *J. Am. Chem. Soc.* **2012**, *135*, 456.
(39) Panman, M. R.; Bodis, P.; Shaw, D. J.; Bakker, B. H.; Newton, A. C.; Kay, E. R.; Leigh, D. A.; Buma, W. J.; Brouwer, A. M.; Woutersen, S. *Phys. Chem. Chem. Phys.* **2012**, *14*, 1865.
(40) Coskun, A.; Spruell, J. M.; Barin, G.; Dichtel, W. R.; Flood, A. H.; Botros, Y. Y.; Stoddart, J. F. *Chem. Soc. Rev.* **2012**, *41*, 4827.
(41) Nygaard, S.; Hansen, C. N.; Jeppesen, J. O. *J. Org. Chem.* **2007**, *72*, 1617.
(42) Raymo, F. M.; Houk, K. N.; Stoddart, J. F. *J. Am. Chem. Soc.* **1998**, *120*, 9318.
(43) Asakawa, M.; Ashton, P. R.; Balzani, V.; Credi, A.; Mattersteig, G.; Matthews, O. A.; Montalti, M.; Spencer, N.; Stoddart, J. F.; Venturi, M. *Chem.—Eur. J.* **1997**, *3*, 1992.
(44) Lau, J.; Blanchard, P.; Riou, A.; Jubault, M.; Cava, M. P.; Becher, J. *J. Org. Chem.* **1997**, *62*, 4936.
(45) Gibson, H. W.; Lee, S. H.; Engen, P. T.; Lecavalier, P.; Sze, J.; Shen, Y. X.; Bheda, M. *J. Org. Chem.* **1993**, *58*, 3748.
(46) Anelli, P. L.; Ashton, P. R.; Ballardini, R.; Balzani, V.; Delgado, M.; Gandolfi, M. T.; Goodnow, T. T.; Kaifer, A. E.; Philp, D.; Pietrazkiwicz, M.; Prodi, L.; Reddington, M. V.; Slawin, A. M. Z.; Spencer, N.; Stoddart, J. F.; Vicent, C.; Williams, D. J. *J. Am. Chem. Soc.* **1992**, *114*, 193.
(47) Material and methods are available in Supporting Information
(48) Connelly, N. G.; Geiger, W. E. *Chem. Rev.* **1996**, *96*, 877.
(49) Jeppesen, J. O.; Nygaard, S.; Vignon, Scott A.; Stoddart, J. F. *Eur. J. Org. Chem.* **2005**, *2005*, 196.
(50) A comparison of the ^{1}H NMR spectra of the dumbbell $\mathbf{D}_S$ and the oxidized dumbbell $\mathbf{D}_S^{2+}$ shows that the SMe groups attached to the TTF unit experience a downfield shift ($\Delta\delta$ = 0.35 ppm) in their resonances upon formation of TTF^{2+}.
(51) Tseng, H.-R.; Vignon, S. A.; Stoddart, J. F. *Angew. Chem., Int. Ed.* **2003**, *42*, 1491.
(52) Tseng, H.-R.; Vignon, S. A.; Celestre, P. C.; Perkins, J.; Jeppesen, J. O.; Fabio, A. D.; Ballardini, R.; Gandolfi, M. T.; Venturi, M.; Balzani, V.; Stoddart, J. F. *Chem.—Eur. J.* **2004**, *10*, 155.
(53) Detailed description of the synthesis can be found in Supporting Information
(54) Nygaard, S.; Hansen, S. W.; Huffman, J. C.; Jensen, F.; Flood, A. H.; Jeppesen, J. O. *J. Am. Chem. Soc.* **2007**, *129*, 7354.
(55) Fahrenbach, A. C.; Barnes, J. C.; Li, H.; Benítez, D.; Basuray, A. N.; Fang, L.; Sue, C.-H.; Barin, G.; Dey, S. K.; Goddard, W. A.; Stoddart, J. F. *Proc. Natl. Acad. Sci. U.S.A.* **2011**, *108*, 20416.
(56) Nijhuis, C. A.; Ravoo, B. J.; Huskens, J.; Reinhoudt, D. N. *Coord. Chem. Rev.* **2007**, *251*, 1761.
(57) Flood, A. H.; Kaifer, A. E. In *Supramolecular Chemistry: From Molecules to Nanomaterial*; John Wiley and Sons, Inc.: New York, 2012; p 451.
(58) Bard, A. J.; Faulkner, L. R. *Electrochemical Methods: Fundamentals and Applications*, 2nd ed.; John Wiley and Sons, Inc.: New York, 2001.
(59) Nygaard, S.; Laursen, B. W.; Hansen, T. S.; Bond, A. D.; Flood, A. H.; Jeppesen, J. O. *Angew. Chem., Int. Ed.* **2007**, *46*, 6093.
(60) Wang, C.; Cao, D.; Fahrenbach, A. C.; Grunder, S.; Dey, S. K.; Sarjeant, A.; Stoddart, J. F. *Chem. Commun.* **2012**, *48*, 9245.
(61) Menzer, S.; White, A. J. P.; Williams, D. J.; Bělohradský, M.; Hamers, C.; Raymo, F. M.; Shipway, A. N.; Stoddart, J. F. *Macromolecules* **1998**, *31*, 295.
(62) Jeppesen, J. O.; Nielsen, K. A.; Perkins, J.; Vignon, S. A.; Fabio, A. D.; Ballardini, R.; Gandolfi, M. T.; Venturi, M.; Balzani, V.; Becher, J.; Stoddart, J. F. *Chem.—Eur. J.* **2003**, *9*, 2982.
(63) Saha, S.; Flood, A. H.; Stoddart, J. F.; Impellizzeri, S.; Silvi, S.; Venturi, M.; Credi, A. *J. Am. Chem. Soc.* **2007**, *129*, 12159.
(64) Hansen, S. W.; Stein, P. C.; Sørensen, A.; Share, A. I.; Witlicki, E. H.; Kongsted, J.; Flood, A. H.; Jeppesen, J. O. *J. Am. Chem. Soc.* **2012**, *134*, 3857.
(65) For simplicity, a positive charge has been placed on one of the dithiole rings and a radical on the other dithiole ring in the radical cation states of the oxidized TTF unit throughout the scheme. However, in general, it is believed that the TTF radical cation is fully conjugated, and consequently both 1,3-dithiole rings are equivalent; therefore, one cannot distinguish the "radical half" or "cation half".